DETERMINATION OF THE TURBULENT ENERGY DISSIPATION RATE FROM LIDAR SENSING DATA

V.A. Banakh and I.N. Smalikho

Institute of Atmospheric Optics,
Siberian Branch of the Russian Academy of Sciences, Tomsk
Received January 9, 1997

In this paper we describe lidar sensing techniques for determining the dissipation rate of turbulent energy using a cw Doppler lidar, based on extracting information on the measured characteristics from: a) the Doppler spectrum width; b) temporal structure functions and from time spectra of the measured rate fluctuations; c) spatial structure function of the rate computed using lidar data obtained when conically scanning about vertical axis with the laser beam. The potentials of the above techniques for reconstructing the profiles of the dissipation rate in the atmospheric boundary layer are analyzed. We compared the results of reconstruction of altitude profiles of the dissipation rate from the Doppler lidar data by different methods as well as with the available data of direct measurements.

1. INTRODUCTION

Determination of the turbulent kinetic energy dissipation rate ε_T from remote sensing data has certain advantages compared to direct techniques by providing high spatial and time resolution of measurements. For these purposes the radars and sodars are commonly used.[1,2,9–14] The majority of the techniques currently in use are based on the relations following from the Kolmogorov and Obukhov laws of turbulent energy transformation in the inertial interval of the inhomogeneity scales.[3–8]

As is seen from the results of theoretical and experimental investigations of the lidar return power spectra of Doppler lidars, it is possible to determine ε_T also from the data obtained using Doppler laser anemometers.[15–29] In this case the dissipation rate can be found from the results of measurements of structure functions and wind velocity fluctuations spectra whose shape in the inertial interval of wave numbers is determined by the $\langle 2/3 \rangle$ or $\langle -5/3 \rangle$ laws, respectively. However, as opposed to the point and low-inertia instruments,[3–8] in the measurements using Doppler anemometers the data on wind velocity are detained from a large volume. For obtaining unbiased estimate ε_T from the structure function or wind velocity spectrum a correct account for averaging of wind velocity fluctuations in sensing volume is needed. The dissipation rate may also be determined from measurements of the Doppler lidar return power spectrum width provided that the dimensions of volume sounded do not exceed the maximum value of wind inhomogeneities in the turbulent inertial interval.[12,21,26,27]

This paper presents a comparative analysis of the techniques for determining turbulent energy dissipation rate using a Doppler cw lidar from the Doppler spectrum width, time structure functions and time spectra of the dissipation rate fluctuations and, finally, spatial structure functions of the rate calculated based on the lidar sensing data obtained at conical scanning with laser beam about vertical axis. We analyze the feasibilities of using these techniques for reconstructing the profiles of ε_T in the atmospheric boundary layer. We compare the results of reconstruction of the profiles of dissipation rate from the Doppler lidar data, using different techniques, with the known results of measurement of $\varepsilon_T(h)$ by the detectors located on a meteorological mast.

2. POWER SPECTRUM OF THE DOPPLER LIDAR RETURN

In operation of a cw Doppler lidar a sounding laser pulse is focused at a distance R from the receiving-transmitting telescope. The radiation, scattered by aerosol particles, is collected using a telescope and then it is mixed with a reference beam on a photodetector. In this case the reference beam and the sounding beam have the same wavelengths. It is essential that the lidar circuit design allows obtaining of the best agreement between the reference beam wavefront with the wavefronts scattered by particles that are in the vicinity of the focus, and in so doing allows the shaping of the final scattering volume. Using a set of narrow-band filters we make the filtration of a received signal. Then the amplitudes or squares of amplitudes of a filtered signal are averaged over some period to obtain the spectrum estimate. The measured power spectrum of a recorded signal will have a useful component (Doppler spectrum), for which, taking into account

0235-6880/97/04–05 295-08 $02.00

the conditions realized, we have

$$\tau_k \ll 1/\Delta f \ll t_0 , \quad t_0 \ll \tau_V ,$$

where τ_k is the correlation time of a scattered wave field (~10^{-6} s), Δf is the frequency resolution (~10^4 Hz), t_0 is the time of averaging when obtaining the spectrum (~10^{-3}–10^{-1} s), and τ_V is the correlation time of wind velocity (~10 s); on the basis of the results from Ref. 2 a simple, suitable for further analysis expression can be derived

$$W(t, f) = S \int_0^\infty dz\, Q_s(z)\, \delta\left(f - \frac{2}{\lambda} V_r(z, t)\right), \qquad (1)$$

where $S(t) = \int_{-\infty}^{+\infty} df\, W(t, f)$ is the signal power, λ is the radiation wavelength, $V_r(z, t)$ is the radial component of wind velocity at the distance z from the lidar, $\delta(x)$ is the Dirac delta-function,

$$Q_s(z) = \{\pi k\, a_0^2\, [(1 - z/R)^2 + z^2/(k\, a_0^2)^2]\}^{-1}$$

is the function characterizing the spatial resolution, $k = 2\pi/\lambda$, a_0 is the radius of a sensing beam in the telescope plane, and R is the focal length of a sensing beam.

For an acceptable spatial resolution the following condition must be fulfilled:

$$k\, a_0^2 \gg R . \qquad (2)$$

In this case we can consider that approximately $\int_0^\infty dz Q_s(z) = 1$, and the maximum of Q_s is at the point $z = R$. Then, having determined the longitudinal size of a volume sounded as $\Delta z = Q_s^{-1}(R)$ we have[24–26,30]

$$\Delta z = (\lambda/2)\, (R^2/a_0^2) . \qquad (3)$$

It is clear that within the framework of the condition (2) with the increase of R, along with an increase in distance from the lidar the increase in Δz is observed.

In the case of a homogeneous flux (V_r = const) the Doppler spectrum W differs from zero only at the frequency $f = (2/\lambda)V_r$ (the Doppler formula). In the atmosphere the wind velocity V_r is inhomogeneous. If in Eq. (1) substitution is made $V = (\lambda/2)\, f$, then the spectrum W represents the lidar return power distribution function over radial velocities V of particles in the volume sounded. The mean value of these velocities $V_D(t)$ and the width square of the velocity distribution function (the square of the Doppler spectrum width in m^2/s^2) $V_s^2(t)$ can be estimated using the formulas

$$V_D(t) = \frac{\lambda}{2} \int_{-\infty}^{+\infty} df\, f\, W(t, f) / S , \qquad (4)$$

$$V_s^2(t) = \left(\frac{\lambda}{2}\right)^2 \int_{-\infty}^{+\infty} df \left[f - \frac{2}{\lambda} V_D(t)\right]^2 W(t, f) / S . \qquad (5)$$

Having substituted Eq. (1) into Eqs. (4) and (5) we have

$$V_D(t) = \int_0^\infty dz\, Q_s(z)\, V_r(z, t) , \qquad (6)$$

$$V_s^2(t) = \int_0^\infty dz\, Q_s(z)\, V_r^2(z, t) - V_D^2(t) . \qquad (7)$$

It is assumed that the wind velocity is statistically stationary and homogeneous. Then for the average over the ensemble Doppler estimate of the velocity and the spectrum width square from Exprs. (6) and (7) we find that $\langle V_D \rangle = \langle V_r \rangle$ and $\sigma_s^2 = \langle V_s^2 \rangle = \sigma_r^2 - \sigma_D^2$, (where σ_s^2 represents the difference between $\sigma_r^2 = \langle V_r^2 \rangle - \langle V_r \rangle^2$, the variance of radial velocity at a fixed point, and $\sigma_D^2 = \langle V_D^2 \rangle - \langle V_D \rangle^2$, the variance of radial velocity averaged over the sounded volume.

When $\Delta z \ll L_V$ where L_V is the outer scale of turbulence, for σ_s^2 the relationship[24,26] takes place

$$\sigma_s^2 = C\, (2/\pi)^{2/3}\, (\varepsilon_T\, \Delta z)^{2/3} , \qquad (8)$$

where $C \approx 2$ is the Kolmogorov constant. Thus, upon the averaging the values of V_s^2 determined from separate measurements of Doppler spectra one can estimate the turbulent energy dissipation rate ε_T using Eq. (8).

The dissipation rate can also be determined from the square of the Doppler spectrum width averaged over the ensemble. Having substituted $V' = (\lambda/2)f - V_D(t)$ for every measured spectrum, for the averaged normalized spectrum $W_a(V') = \left\langle \frac{2}{\lambda} W\left[t, \frac{2}{\lambda}(V' + V_D(t))\right] / S \right\rangle$ we find from Eq. (1)

$$W_a(V') = \int_0^\infty dz\, Q_s(z) \langle \delta(V' - \Delta V) \rangle , \qquad (9)$$

where $\Delta V = V_r(z, t) - V_D(t) =$

$$= \int_0^\infty dz'\, Q_s(z') \times [V_r(z, t) - V_r(z', t)].$$

Having averaged over ΔV in Eq. (9) with the probability density $P(\Delta V, z)$, depending in the general case on the coordinate z, we derive the expression

$W_a(V') = \int_0^\infty dz\, Q_s(z)\, P(V', z)$. At large sounding volumes ($\Delta z >> L_V$) the rate being determined is greatly averaged so that $V_D \approx \langle V_r \rangle$. Consequently, in this case the difference $\Delta V \approx V_r(z, t) - V_D(t)$ is the fluctuating part of the radial rate $\Delta V \approx V_r(z, t) - \langle V_r \rangle$. It is known that in the atmosphere the wind velocity fluctuations have Gaussian distribution. Therefore at $\Delta z >> L_V$ the probability density P is Gaussian and due to statistical homogeneity of wind velocity fluctuations, P does not depend on z. So in this case the spectrum $W_a(V') \equiv P(V')$ is of Gaussian distribution shape, its width is determined by the wind velocity variance in the atmosphere σ_r^2 and does not contain the information on ε_T .[26,28]

Let us consider the moments of centered relatively V_D the value of the rate V':

$$M_n = \int_{-\infty}^{+\infty} dV'\, V'^n\, W_a(V') \,. \qquad (10)$$

From (9) and (10) we have $M_n = \int_0^\infty dz\, Q_s(z) \langle [V_r(z, t) - V_D(t)]^n \rangle$ from where it is not difficult to find that $M_0 = 1$, $M_1 = 0$ and $M_2 = \sigma_s^2$. For obtaining the multipole moments we must know the probability density $P(\Delta V, z)$. If we assume that it obeys normal distribution law, then for $\Delta z << L_V$ it is shown that $M_4 \neq 3M_2^2$. Hence, in the general case, the distribution $W_a(V')$ differs from the normal one.

Figure 1 shows the measurement results on $W_a(V')$ for the case of $\Delta z << L_V$ (solid curve *2*). When averaging 2500 Doppler spectra measured during $t_0 = 50$ ms were used. Here the functions $(\sqrt{2p}\sigma_s)^{-1} \exp\{(-V'^2/(2\sigma_s^2)\}$ are presented by dashed curves, where σ_s^2 denotes the squares of measured (averaged) spectral widths. If in the case of $\Delta z > L_V$ the measured spectrum is of Gaussian distribution then at $\Delta z << L_V$ the excess coefficient $M_4/M_2^2 - 3 \neq 0$ and is positive. For the data shown in Fig. 1 the excess coefficient equals unity.

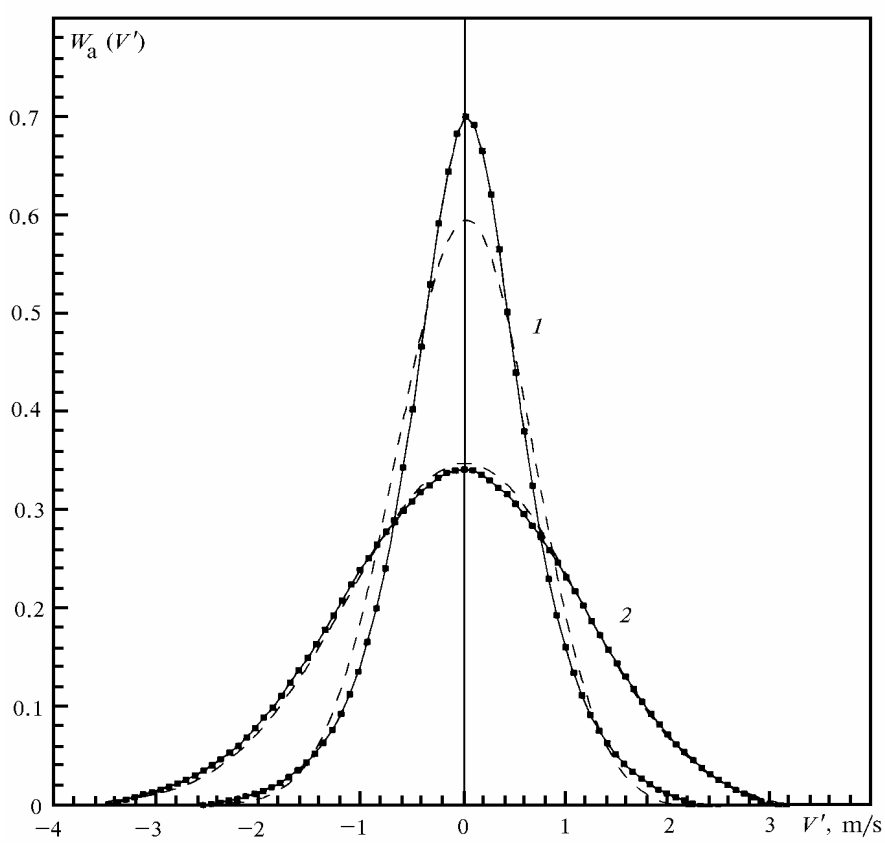

FIG. 1. The normalized Doppler spectrum $W_a(V')$ at $\Delta z \ll L_V$ (curve 1) and at $\Delta z > L_V$ (curve 2).

As the experience of the experimental data processing shows the estimates of ε_T should better be made from the width of the averaged spectrum $W_a(V')$ since in this case the fluctuations of the noise component are essentially averaged that simplifies the isolation of a useful spectral component. The turbulent energy dissipation rate ε_T can be determined from the Doppler spectrum width σ_s only at small, as compared with the outer scale of turbulence, longitudinal dimensions of sounding volume ($\Delta z << L_V$). With the

increase of sounding distance R in the case of a ground-based lidar this condition will be violated because of the increase in Δz (see (3)). Consequently, this method has certain restrictions on the altitude of measurements ε_T. In particular, for CO_2 lidar when the telescope diameter is 30 cm, this method can be used for sounding ε_T only in the atmospheric boundary layer ($h \le 100$–150 m).

3. TIME BEHAVIOR OF WIND VELOCITY MEASURED USING A DOPPLER LIDAR

One of the methods, which under certain conditions enables us to increase the sounding distance, is that which for determining ε_T from the time behavior of the wind velocity

$$S_D(f) = 2 \int_{-\infty}^{+\infty} d\tau \, \langle V'_D(t+\tau)\, V'_D(t)\rangle \exp(-i\,2\pi f \tau) \qquad (11)$$

where $V'_D = V_D - \langle V_D \rangle$, $f \ge 0$. By substituting Eq. (6) into Expr. (11) and using the hypothesis of "frozen" turbulence we have

$$V_r(z, t) = U_z(z + \cos\gamma\, U\, t,\ \sin\gamma\, U\, t,\ 0,\ 0)\,, \qquad (12)$$

where $U_z(z, x, y, t)$ is the projection of the wind velocity vector on the axis parallel to the beam axis at a point $\{z, x, y\}$ of Cartesian coordinates, U is the mean wind velocity, and γ is the angle between the wind direction and the beam axis. In Ref. 26 for the frequency range $f \gg U/L_V$ the following expression was obtained:

$$S_D(f) = S_z(f)\, H(f)\,, \qquad (13)$$

where $S_z(f) = C_2 \left[1 + \frac{1}{3}\sin^2\gamma\right] \varepsilon_T^{2/3}\, U^{2/3}\, f^{-5/3}$

is the time behavior of the zth component of wind velocity at a fixed point ($z = R$), $C_2 \approx 0.15$,

$$H(f) = C_3 \left(1 + \frac{1}{3}\sin^2\gamma\right)^{-1} \int_{-\infty}^{+\infty} d\xi\, (1+\xi^2)^{-4/3} \times$$
$$\times \left[1 - \frac{8}{11}\frac{(\cos\gamma - \xi\sin\gamma)^2}{1+\xi^2}\right] \times$$
$$\times \exp\left\{-\frac{4Dz\, f}{U}\,|\cos\gamma - \xi\sin\gamma|\right\}$$

is the transmission function of a low-frequency filter, $C_3 = (55/27)[\Gamma(1/3)\Gamma(11/6)]/(4\pi^{1/2})$. Under conditions when the turbulence "freezing" hypothesis is valid we can determine ε_T from the measured spectrum of $S_D(f)$ using formula (13) for any sounding distance R satisfying the inequality (2). Necessary information on γ and U can be obtained from the data of additional lidar measurements at conical scanning. In the limiting case of large Δz we have from (13)

$$S_D(f) = C_4\, \varepsilon_T^{2/3}\, |U\sin\gamma|^{5/3}\, (1/\Delta z)\, f^{-8/3}\,, \qquad (14)$$

where $C_4 = C_2 C_3/2 \approx 0.06$.

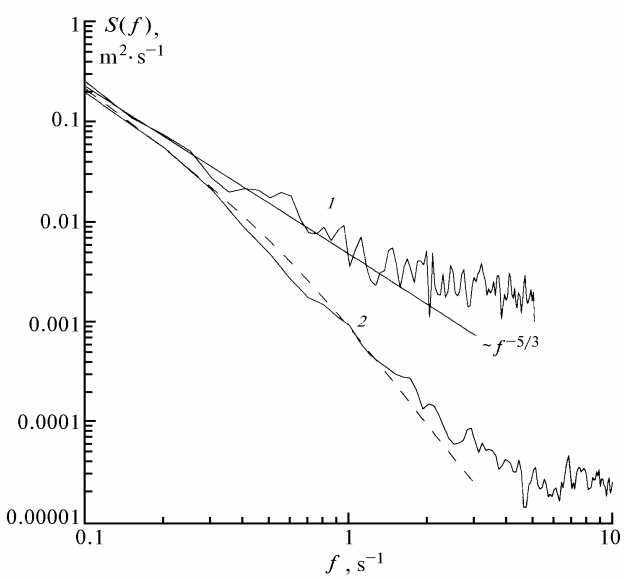

FIG. 2. The wind velocity ranges measured using an acoustic anemometer (1) and a Doppler lidar (2); the calculation by Eq. (13) is shown by the dashed curve.

Figure 2 presents the results of simultaneous measurements of time behaviors of wind velocity using an acoustic anemometer (which can conditionally be considered to be a point meter) and the Doppler lidar with $\Delta z = 2.3$ m at a height $h = 7$ m. The calculation by formula (13) is presented by dashed line where for ε_T, γ, and U the data of an acoustic anemometer are used. The figure shows the influence of spatial averaging over a sounded volume (low-frequency filtration) on the wind velocity variation measured using a Doppler lidar.

Experimental verification of Eq. (14) is given in Ref. 31 at a strong side wind (relative to the axis of sounding beam). However, as the experiments, performed at a weak side wind and large Δz, show the measured dependence of time behavior on the frequency is not described by Eq. (14), that is connected with the violation of the conditions of applicability of "frozen" turbulence hypothesis. This drawback of the method does not enable one to obtain the estimates of ε_T for large values of Δz at a light breeze, and, hence, for long sounding paths R.

4. STRUCTURE FUNCTION OF WIND VELOCITY ESTIMATED FROM THE SCANNING LIDAR DATA

The Doppler lidar with a scanning drive makes it possible, during measurements, to rapidly change the sounding volume in space. In this case the turbulent inhomogeneities of wind flux are

considered to be always "frozen". The method for the determination of ε_T from the data of conical scanning lidar is based on the use of this fact.

In Ref. 29 one may find a diagram of sounding geometry with the Doppler lidar at conical scanning. The azimuth angle of scanning is denoted by θ, the elevation angle of sounding beam is denoted by φ. In the course of scanning at an angular velocity ω_0 in equal intervals $t_0 = \Delta\theta/\omega_0$, where $\Delta\theta$ is the azimuth angle between the adjacent readings, the Doppler variations of the lidar returns are measured. Based on these measurements the radial velocity $V_D(\theta)$ in the direction of azimuth angle θ is estimated. Then we calculate the structure function $D(\theta_1, \theta_2) = \langle[\tilde{V}_D(\theta_1) - \tilde{V}_D(\theta_2)]^2\rangle$, where $\tilde{V}_D$ denotes the deviations of V_D from the averaged over the entire range of scanning Doppler estimate of the radial wind velocity. In Ref. 29 for this function we obtained the following formula:

$$D(\theta_1 - \theta_2) = \int_0^\infty\int dz_1\, dz_2\, Q_s(z_1)\, Q_s(z_2) \times$$

$$\times \left\{ [(z_1 - z_2)^2 + (\theta_1 - \theta_2)^2 z_1 z_2 \cos^2\varphi]^{1/3} \times \right.$$

$$\times \left[1 + \frac{1}{3} \frac{(\theta_1 - \theta_2)^2 z_1 z_2 \cos^2\varphi}{(z_1 - z_2)^2 + (\theta_1 - \theta_2)^2 z_1 z_2 \cos^2\varphi} \right] -$$

$$\left. - |z_1 - z_2|^{2/3} \right\} C\, \varepsilon_T^{2/3}, \qquad (15)$$

where the angles θ_1 and θ_2 are given in radians and $|\theta_1 - \theta_2| \ll \pi/2$.

At $\Delta z \to 0$ Eq. (15) takes the form

$$D(\theta_1 - \theta_2) = (4/3)\, C\, \varepsilon_T^{2/3} (|\theta_1 - \theta_2|\, R \cos\varphi)^{2/3} \qquad (16)$$

for the transverse structure function of the wind velocity.[3] From this we calculate the condition of applicability of Eq. (15): the length of sector arc on the base of the scanning cone $|\theta_1 - \theta_2| R\cos\varphi$ must not exceed the size of the largest inhomogeneity in the inertial interval, i.e.,

$$|\theta_1 - \theta_2|\, R \cos\varphi \ll L_V\,. \qquad (17)$$

Thus, from the results of measurements of the structure function $D(\theta_1 - \theta_2)$ one can estimate, using Eq. (15), the value of the turbulent energy dissipation rate ε_T in the angle range $|\theta_1 - \theta_2|$, satisfying the inequality (17). In this method the only limitation on the sounding for ε_T is the condition (2), when for the lidar at $\lambda = 10.6$ μm and 30 cm telescope diameter the sounding distance R can be 1 km.

As an example the points in Fig. 3 indicate the function $D(\theta)$ obtained experimentally. The results of calculations of $D(\theta)$ using Eqs. (15) and (16) are given by solid and dashed curves, respectively, where the estimate of ε_T from the experimental function $D(\theta)$ is used. The difference in the calculated curves characterizes the degree of influence of spatial averaging of wind velocity fluctuations along a sounding beam axis.

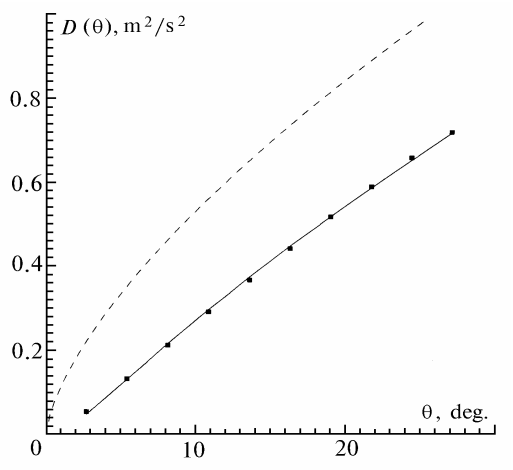

FIG. 3. Structure function of wind velocity measured with a scanning Doppler lidar: the experimental data are denoted by squares; the calculated data are denoted by solid and dashed curves, by Eqs. (15) and (16), respectively.

5. RESULTS OF RECONSTRUCTION OF ALTITUDE PROFILES OF THE DISSIPATION RATE

For the purpose of reconstruction of the dissipation rate altitude profile from the data of a cw Doppler lidar the measurements may be performed successively at fixed altitudes h_i (i = 1, 2, 3...). For obtaining statistically stable estimates of $\varepsilon_T(h_i)$ the measurements can be repeated. The value ε_T can be estimated from the Doppler spectrum width from the measurements both a fixed position of a sounding beam and at scanning. When we evaluate ε_T from the time dependence of wind velocity the sounding beam remains stationary during the entire period of time at the altitude h_i.

We have selected the experimental data obtained with the use of a cw CO_2 Doppler lidar of the Institute of Optoelectronics of the German Aerospace Agency at different wind velocities. The results of reconstruction of altitude profiles of ε_T from the above data are given in Fig. 4 as the marks connected by solid lines and correspond to the measurements at different altitudes of σ_s^2 (*1*, *2*), $S_D(f)$ (*3*) and $D(\theta)$ (*4*, *5*, *6*). The profiles *1* and *5* are obtained at a weak breeze ($U < 3$ m/s), and *2*, *3*, *4* and *6* profiles are obtained at a strong wind ($U > 10$ m/s). Relative random errors of the estimates are 15–20%.

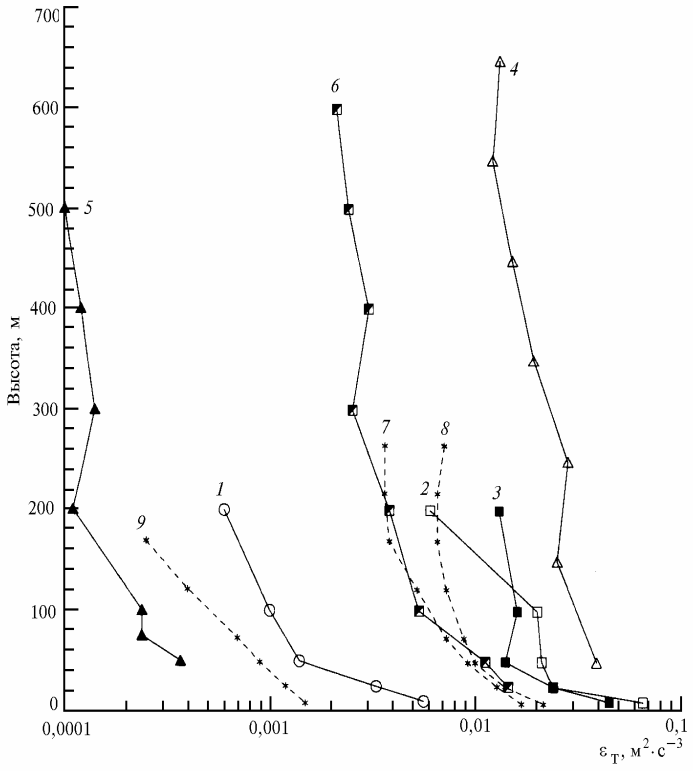

FIG. 4. Altitude profiles of the dissipation rate of turbulent energy reconstructed from the data of the Doppler lidar (1–6) and the measurements on a meteorological mast (7–9). Curves 1 and 2 denote the result of reconstruction of $\varepsilon_T(h)$ *from* σ_s^2, *3 – from* $S_D(f)$ *and (4–6) – from* $D(\theta)$.

Weather conditions during the measurements of the profiles *2–4* were characterized by a gusty wind and strong turbulence (measurements were carried out before the rain) that can explain relatively large values of ε_T, observed in these experiments. The profile *5*, on the contrary, was measured at weak breeze with the velocity no more than 1.5 m/s, and weak turbulence. As a rough approximation, we can consider that ε_T is proportional to the cube of mean wind velocity.[3–6] At such a breeze small values of ε_T can be observed.

Of some interest is the comparison of the results obtained using different methods. The profiles *2* and *3* are reconstructed from the same data. We notice that except for the top level the methods present similar results. The estimate of ε_T from σ_s^2 at the height $h = 200$ m was obtained when the size of sounding volume $\Delta z = 100$ m, exceeding the maximum size of turbulent inhomogeneities in the inertial interval, that must result in understating of the estimated value ε_T. A comparison of the profiles reconstructed from analogous data a weak breeze (curve *1*) shows that up to the height $h = 50$ m (the size of Δz is small) the estimates of ε_T from σ_s^2 and $S_D(f)$ differ within the limits of random error. Above this level the estimates of ε_T from $S_D(f)$ become essentially overestimated that is connected with their shift due to inapplicability of frozen turbulence hypothesis.

For a comparison Fig. 5 shows the results of reconstruction of the profiles of $\varepsilon_T(h)$ from one and the same data on σ_s^2 (curve *1*) and $D(\theta)$ (curve *2* corresponds to curve *5* in Fig. 4). It is evident that at lower levels the methods give much close results. However, at high altitudes the values of ε_T obtained from σ_s^2 are understated because of the excess of Δz over maximum size of turbulent inhomogeneities in the inertial interval. In particular, for the height $h = 500$ m the estimate of ε_T from σ_s^2 is understated as compared with the value obtained from $D(\theta)$ by a factor of five. The same difference is observed when comparing the profiles of $\varepsilon_T(h)$ obtained from σ_s^2 with those obtained from $D(\theta)$ and presented in Fig. 4 as the curves *4* and *6*. The comparisons of the results of simultaneous measurements of ε_T using the Doppler lidar and the acoustic anemometer at $h = 7$ m showed a good agreement of the data obtained (in particular, see Table in Ref. 27 and Fig. 2 in this paper). Figure 4 presents the results published in Ref. 32 of measurements at a meteorological mast indicated by dashed curves *7*, *8*, and *9*. Curve *7* corresponds to the case of measurements at neutral stratification, curve *8* – at unstable stratification and curve *9* – at stable stratification. The Doppler lidar data presented in Fig. 4 were obtained from the measurements in the fall at daytime at neutral and close to it stratification. The conditions under which the measurements were carried out and the results of their processing presented

by curve *6*, completely correspond to the conditions of neutral stratification. The figure shows that these data are in a good agreement with the results of direct measurements (curve *7*).

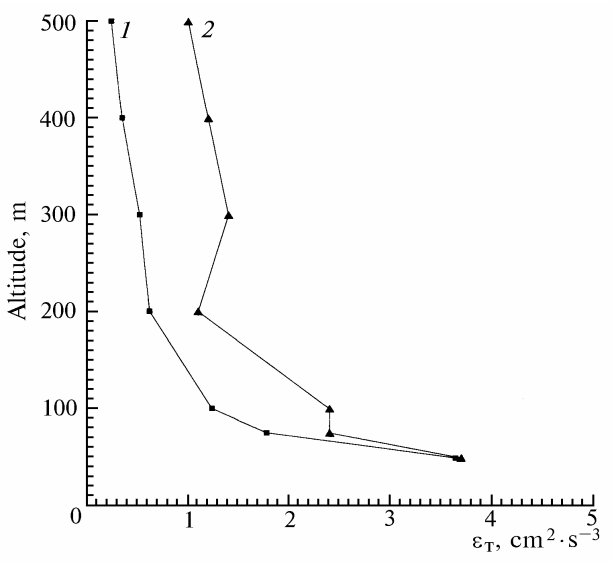

FIG. 5. Results of reconstruction of altitude profiles of the dissipation rate from the data of the scanning lidar when estimating ε_T *from* σ_s^2 *(1) and from* $D(\theta)$ *(2).*

CONCLUSION

This paper describes the potentialities of the turbulent energy dissipation rate measurement with a cw Doppler lidar. Three sensing techniques for determining ε_T have been considered, namely, from a Doppler lidar return power spectrum width from the temporal spectrum of wind velocity and from the structure function estimated from the data of a scanning lidar. All these techniques show a common feature, i.e., estimating ε_T from the corresponding statistical characteristics of turbulent variations of wind velocity in the inertial spectral interval taking into account spatial averaging over the volume sounded. When using the first and third technique we deal with the spatial turbulent structure, and when using the second technique we deal with the spatiotemporal turbulent structure that causes the need for model setting of spatiotemporal correlation function of wind velocity. As the results of investigations show, in the case of large longitudinal dimensions of the volume sounded the use of the hypothesis of frozen turbulence for setting the spatiotemporal correlation function in case of a weak lateral breeze is unsuitable. The main drawback of the first method is the limitation on the longitudinal size of the sounded volume and, hence, on the distance (height) of sounding. These limitations are not pertinent to the third method.

The methods developed enable us to reconstruct the altitude profiles of the turbulent energy dissipation rate from the data of a cw Doppler lidar practically along the whole altitude of the atmospheric boundary layer. The results obtained in this case do not contradict known experimental data on the altitude variation and absolute values of ε_T that may serve as a proof of the applicability of these methods.

ACKNOWLEDGMENT

The authors wish to acknowledge the important contribution of Dr. Ch. Werner from the Institute of Optoelectronics of German Aerospace Agency for giving us the experimental data obtained with the lidar of the Institute of Optoelectronics.

The work has been supported by the Russian Foundation for Basic Research (grant N 94–05–16601–a).

REFERENCE

1. R.J. Doviak and D.S. Zrnic , *Doppler Radar and Weather Observations* (Academic Press, 1993), 562 pp.
2. N.P. Krasnenko, *Acoustic Sounding of the Atmosphere* (Nauka, Novosibirsk, 1986), 166 pp.
3. J. Lamli and G. Panovskii, *Structure of Atmospheric Turbulence* (Mir, Moscow, 1966), 264 pp.
4. A.S. Monin and A.M. Yaglom, *Statistical Hydromechanics*, Part 2 (Nauka, Moscow, 1967), 720 pp.
5. S.S. Zilitinkevich, *Dynamics of the Atmospheric Boundary Layer* (Gidrometeoizdat, Leningrad, 1970), 290 pp.
6. N.L. Byzova, V.N. Ivanov, and E.K. Garger, *Turbulence in the Atmospheric Boundary Layer* (Gidrometeoizdat, Leningrad, 1989), 263 pp.
7. N.K. Vinnichenko, N.Z. Pinus, S.M. Shmeter, and G.N. Shur, *Turbulence in a Free Atmosphere* (Gidrometeoizdat, Leningrad, 1976), 287 pp.
8. T.R. Oke, *Climates of the Atmospheric Boundary Layer* (Gidrometeoizdat, Leningrad, 1982), 359 pp.
9. A.R. Bohne, J. Atmos. Science **39**, 1819–1837 (1982).
10. W.K. Hocking, J. Atmos. and Terr. Physics **45**, Nos. 2–3, 89–102 (1983).
11. W.K. Hocking, Radio Science **20**, No. 6, 1403–1422 (1985).
12. K.A. Brewster and D.S. Zrnic, J. Atmos. Oceanic Technol. **3**, 440–452 (1986).
13. S.A. Cohn, J. Atmos. Oceanic Technol. **12**, 85–95 (1995).
14. L. Eymard and A. Weill, J. Appl. Meteorol. **21**, No. 12, 1891–1906 (1982).
15. F. Köpp, R.L. Schwiesow, and Ch. Werner, J. Climate Appl. Meteorol. **3**, No. 1, 148–151 (1984).
16. J.G. Hawley, et al., Appl. Opt. **32**, 4557–4568 (1983).
17. R.J. Keeler, et al., J. Atmos. Oceanic Technol. **4**, 113–127 (1987).

18. G.M. Ancellet, R.I. Menzies, and W.B. Grant, J. Atmos. Oceanic Technol. **6**, No. 1, 50–58 (1989).
19. T. Gal-Chen, Xu Mei, and W.L. Eberhard, J. Geophys. Res. **97**, No. D17, 18409–18423 (1992).
20. F. Köpp et al., Contribution to Atmospheric Physics **67**, No. 4, 269–286 (1994).
21. V.M. Gordienko et al., Optical Engineering **33**, No. 10, 3206–3213 (1994).
22. R.G. Frehlich, S.M. Hannon, and S.W. Henderson, J. Atmos. Oceanic Technol. **11**, 1517–1528 (1994).
23. S.M. Hannon, J.A. Thomson, S.W. Henderson and R.M. Huffaker, *Air Trafic Control Technologies*, Proc. SPIE **2464**, 94–102 (1995).
24. V.A. Banakh, Ch. Werner, F. Köpp, and I.N. Smalikho, *Atmospheric Propagation and Remote Sensing*, Proc. SPIE **1968**, 483–493 (1993).
25. V.A. Banakh, Ch. Werner, F. Köpp, and I.N. Smalikho, Appl. Opt. **34**, 2055–2067 (1995).
26. I.N. Smalikho, Atmos. Oceanic Opt. **8**, No. 10, 788–793 (1995).
27. V.A. Banakh, Ch. Werner, N.N. Kerkis, F. Köpp, and I.N. Smalikho, Atmos. Oceanic Opt. **8**, No. 12, 955–959 (1995).
28. V.A. Banakh, N.N. Kerkis, N.N. Smalikho, F. Köpp, and Ch. Werner, *Coherent Laser Radar. Technical Digest Series* **19**, 116–119 (1995).
29. V.A. Banakh, Ch. Werner, F. Köpp, and I.N. Smalikho, Atmos. Oceanic Opt. **9**, No. 10, 849–854 (1996).
30. C.M. Sonnenschein and F.A. Horridan, Appl. Opt. **10**, No. 7, 1600–1604 (1971).
31. V.A. Banakh, Ch. Werner, F. Köpp, and I.N. Smalikho, Atmos. Oceanic Opt. **10** No. 3, 202–208 (1997).
32. Z.I. Volkovitskaya, V.P. Ivanov, Izv. Akad. Nauk SSSR, Fiz. Atmos. Okeana **6**, No. 5, 435–444 (1970).